Near- and Extended-Edge X-Ray-Absorption Fine-Structure Spectroscopy Using Ultrafast Coherent High-Order Harmonic Supercontinua

Dimitar Popmintchev, Benjamin R. Galloway, Ming-Chang Chen, Franklin Dollar, Christopher A. Mancuso, Amelia Hankla, Luis Miaja-Avila, Galen O'Neil, Justin M. Shaw, Guangyu Fan, Skirmantas Ališauskas, Giedrius Andriukaitis, Tadas Balčiunas, Oliver D. Mücke, Audrius Pugzlys, Andrius Baltuška, Henry C. Kapteyn, Tenio Popmintchev, and Margaret M. Murnane

Phys. Rev. Lett. **120**, 093002 — Published 1 March 2018

DOI: 10.1103/PhysRevLett.120.093002

Near and extended edge X-ray absorption fine structure spectroscopy using ultrafast coherent high harmonic supercontinua

Dimitar Popmintchev[1]*, Benjamin R. Galloway[1], Ming-Chang Chen[2], Franklin Dollar[1], Christopher A. Mancuso[1], Amelia Hankla[1], Luis Miaja-Avila[3], Galen O'Neil[3], Justin M. Shaw[3], Guangyu Fan[4], Skirmantas Ališauskas[4,5], Giedrius Andriukaitis[4], Tadas Balčiunas[4], Oliver D. Mücke[6,7], Audrius Pugzlys[4], Andrius Baltuška[4], Henry C. Kapteyn[1], Tenio Popmintchev[1]*, Margaret M. Murnane[1]*

[1] *JILA, University of Colorado at Boulder, Boulder, CO 80309-0440 USA*
[2] *National Tsing Hua University, Institute of Photonics Technologies, Hsinchu 30013, Taiwan*
[3] *National Institute of Standards and Technology, Boulder, CO 80305, USA*
[4] *Photonics Institute, TU Wien, Gusshausstrasse 27-387, A-1040 Vienna, Austria*
[5] *Deutsches Elektronen-Synchrotron DESY, Notkestraße 85, D-22607 Hamburg, Germany*
[6] *Center for Free Electron Laser Science (CFEL), Deutsches Elektronen-Synchrotron DESY, Notkestraße 85, D-22607 Hamburg, Germany*
[7] *The Hamburg Center for Ultrafast Imaging, Luruper Chaussee 149, 22761 Hamburg, Germany*

Recent advances in high-order harmonic generation have made it possible to use a tabletop-scale setup to produce spatially and temporally coherent beams of light with bandwidth spanning 12 octaves, from the ultraviolet up to X-ray photon energies >1.6 keV. Here we demonstrate the use of this light for X-ray absorption spectroscopy at the K- and L-absorption edges of solids at photon energies near 1 keV. We also report X-ray absorption spectroscopy in the water window spectral region (284-543eV) using a high flux HHG X-ray supercontinuum with *10^9 photons/s in 1% bandwidth*, three orders of magnitude larger than has previously been possible using tabletop sources. Since this X-ray radiation emerges as a single attosecond-to-femtosecond pulse with peak brilliance exceeding *10^{26} photons/s/mrad^2/mm^2 /1% bandwidth*, these novel coherent X-ray sources are ideal for probing the fastest molecular and materials processes on femtosecond-to-attosecond time scales and picometer length scales.

Coherent X-ray spectroscopies are powerful probes of matter, bringing unique advantages that are complementary to visible or infrared spectroscopies. Techniques such as X-ray absorption spectroscopy (XAS) can encode the instantaneous charge and spin state in the X-ray absorption edge structure, giving additional information about the local structure, chemical nature and electronic structure as well as orbital and spin ordering phenomena. In particular, the extreme ultraviolet (EUV) to soft X-ray (SXR) photon energy range from ~40 eV to above 1 keV is particularly relevant for probing bulk materials and interfaces. Examples include oxide materials (through the oxygen K-shell edge at 0.54 keV), or magnetic and superconducting materials (employing spectroscopies at the M- and L-edges). Angle-resolved photoemission spectroscopy (ARPES) can capture the dynamic electronic band structure, while XAS is sensitive to the electronic, spin and geometric structure of molecules and materials. The near-edge X-ray absorption fine structure (NEXAFS) originates from core level transitions to unoccupied states, while the oscillatory structure in the broadband X-ray absorption, called extended X-ray absorption fine structure (EXAFS), results from modulations in the absorption probability caused by photoelectron interferences, which can be used to unambiguously determine the local atomic structure (within 10-20 Å) with picometer resolution using sources with nanometer scale wavelength. Essentially, these techniques provide a label-free, atomic-site-specific spectroscopy technique, since different elements have different characteristic core absorption edges in the soft X-ray region, and their exact positions depend on the local charge environment. Moreover, soft X-rays can penetrate thick or opaque samples.

In comparison with X-ray crystallography, X-ray absorption fine structure (XAFS) employs significantly lower X-ray photon energies, requires a broad or tunable spectrum, probes local atomic distribution, and does not need a crystalline sample. Indeed, XAFS is applicable to various phases of matter (i.e. crystals, gases, low concentration solutions, disordered solids, etc.), making it particularly well suited for probing dynamic processes that generally result in some level of disorder. XAFS can thus provide extensive chemical and structural information about the types of atoms present, their coordination numbers (number of neighboring atoms at particular distances), mean inter-atomic distances, and disorder (using EXAFS), oxidation state, and coordination chemistry (using NEXAFS).

Past implementations of XAFS used both laser plasma emission and synchrotron radiation from large (synchrotrons, Omega, NIF) and also from smaller laser plasma based facilities [1-4]. These incoherent soft X-ray sources typically provide a peak brilliance of less than 10^{26} photons/s/mrad^2/mm^2 /1% bandwidth with time resolution ~1ps [5].

More recently, high harmonic generation (HHG) [6-12] sources have made it possible to implement coherent X-

ray spectroscopies using a tabletop-scale apparatus [13-17]. These sources have unprecedented spatial and temporal coherence and are capable of extending the XAFS technique for measuring dynamics at attosecond-to-femtosecond time scales as well as providing picometer spatial resolution, with elemental and chemical specificity. In the EUV region of the spectrum at photon energies <100 eV, where bright HHG sources have been used for more than a decade, a broad range of applications in nano- and materials science have been demonstrated, including the investigations of how nanoscale energy flow differs from bulk [18, 19], how fast a material can change its electronic or magnetic state [20-22], how fast spin currents control and enhance magnetization in materials [23, 24], and more recently, how the band structure of a material influences photoemission [25]. In the latter case, recent work directly observed the fastest excited-state dynamics to date, measuring an excited state lifetime of ~212±30 attoseconds, for an electron excited ~20 eV above the Fermi level into a resonant transient state, as well as distinguishing attosecond charge scattering and screening in a material [26]. Many of these advances already have made use of the broadband nature of the HHG emission to access dynamics at multiple atomic sites simultaneously - essentially acting as a low-photon energy version of NEXAFS. These results already emphasize that these new sources can uniquely access new regimes for material science, and identify and control quantum processes at the nanoscale.

EXAFS requires absorption data over a broad spectral bandwidth >100 eV, which has only recently become possible [7-12] via HHG sources. When mid-infrared (mid-IR) femtosecond lasers are used to drive HHG, ultra-broad coherent supercontinua are produced, with >1.3 keV tail-to-tail spectral width, spanning many characteristic X-ray edges (Figures 1). Furthermore, mid-IR laser driven HHG exhibits a time-gated phase matching that allows for optimized upconversion while naturally confining the emission to a single isolated attosecond burst [9, 27], and resulting in a true supercontinua. The first pioneering works on EXAFS spectroscopy using tabletop HHG sources used a photon flux of 10^4 photons/s at 1 keV and 10^2 photons/s at 2 keV. Using these sources, static XAFS spectra were acquired at various absorption edges, and a dynamic edge shift with sub-ps resolution was observed in the XAFS spectra [28, 29]. However, the low signal-to-noise ratio (SNR) and long acquisition times in such experiments lead to relatively large uncertainties. As a result, in the past, the large SNR that is required for XAFS measurements meant that large facilities were the only sources suitable for this type of spectroscopy [30, 31].

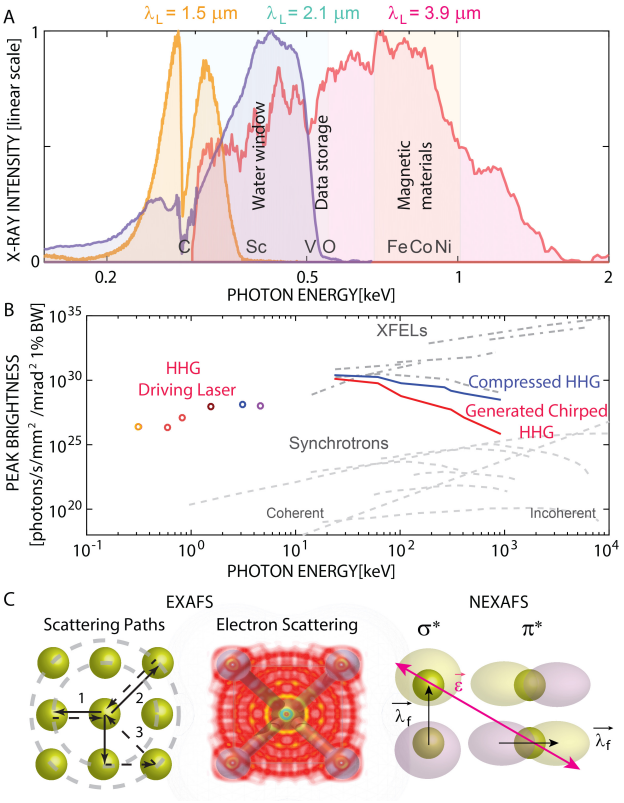

Figure 1. A) Three broadband soft X-ray supercontinua up to 0.36 keV, 0.55 keV, and 1.6 keV photon energies, are generated using mid-IR driving lasers at 1.5 μm , 2.1 μm , and 3.9 μm , respectively, in He gas. **B)** Peak brightness of coherent high-harmonic X-ray sources using UV, visible and IR driving lasers (solid lines). X-ray FELs and synchrotron sources are in dashed lines [32-35] **C)** (left) Illustration showing the scattering paths of photoelectrons from the first (path 1) and second shell (path 2), as well as secondary rescattering (path 3). (center) Photoelectron scattering and interference of the electron-wave packet for a 2D planar lattice. (right) XAFS sensitivity to the polarization $\vec{\varepsilon}$ and final $\vec{\lambda}_f$ orbital direction.

With the development of femtosecond laser sources in the mid-IR, and their application to drive HHG in an optimized, phase-matched configuration, static NEXAFS at the sulfur and carbon edges were demonstrated [13], at the sulfur edge (~163eV) employing a photon flux of ~10^9 photons/s, and at the carbon (C) edge (~282eV) with a flux of 10^7 photons/s in 1% bandwidth [14, 15, 36].

Here we use bright, tabletop, broadband HHG supercontinua for NEXAFS and EXAFS spectroscopies at the K- and L-absorption edges to study the structure and chemistry of solids. Specifically, we demonstrate the first XAFS spectroscopy at the K- and L-absorption edges of solids in the near-keV range using a high harmonic source. We also demonstrate X-ray absorption spectroscopy in the 'water window' spectral region (284-541eV) using an X-ray supercontinuum with high flux *10^9 photons/s in 1%*

bandwidth, which is three orders of magnitude larger than fluxes previously demonstrated [10, 36]. In the future, because this X-ray radiation emerges as a single isolated attosecond-to-femtosecond burst, with peak brilliance exceeding 10^{26} *photons/s/mrad^2/mm^2 /1% bandwidth*, these novel coherent X-ray sources will be ideal for dynamic probing of the fastest processes in molecules and materials on femtosecond-to-attosecond time and picometer length scales.

Two different mid-IR laser systems were used in this work. First, a 14 millijoule (mJ), optical parametric chirped-pulse amplifier (OPCPA) at a wavelength of 3.9 μm with repetition rate of 20 Hz, and 80-fs pulse duration, producing a HHG supercontinuum spanning the EUV and the soft X-ray spectral region up to 1.6 keV (about 7.7 Å) with *~2·10^6 photons/s/mrad^2/mm^2/1% bandwidth* near ~1 keV. Further details of the OPCPA experimental beamline can be found in Ref. [37]. Second, an optical parametric amplifier (OPA) pumped by a 19.5 mJ, 20 fs, 1 kHz repetition rate Ti:Sapphire laser. To avoid any nonlinearity from pulse propagation in air and to maintain excellent beam quality, the 20 fs Ti:Sapphire pulses are stretched in the time domain to >150 fs FWHM and then recompressed to 20 fs using chirped mirrors placed just before each amplification stage of the OPA. This results in excellent beam quality profiles and short few-cycle pulse durations for the mid-IR light. We note that the driving lasers at 2.1 μm and 3.9 μm are derived from the idler beam of a parametric process and are passively CEP (carrier-envelope phase) stable.

The OPA was used to produce a 2.75 mJ idler pulse with duration as short as ~26 fs or four optical-cycles at 2.1 μm and a signal pulse with 4.5 mJ and a ~24 fs, five-cycle pulse duration when centered at 1.5 μm. The driving pulses were focused into a 1-5 cm long waveguide, with inner diameter of 150-400 μm, and filled with ~10-20 atm of helium gas. The generated HHG supercontinuum extends up to photon energies of 550 and 360 eV for the idler and signal beams, respectively (Figure 1A). The high photon flux of *>10^9 photons/s in 1% bandwidth* in the 'water window' spectral region is more than 1000 times larger than previously demonstrated [10, 36]. The estimated HHG flux after the waveguide is summarized in Figure 1B. These bright ultra-broadband HHG pulses with laser-like properties allow us to obtain high-quality EXAFS data, from which picometer-resolution structural information is extracted by accumulating only a small number of laser shots. Moreover, our data show excellent agreement with theory. In our experimental apparatus, the HHG generation setup is followed by an X-ray spectrometer with a spectral resolution of $\lambda/\Delta\lambda$ >1000 (EUV - soft X-ray region), followed by thin metal filters to separate the fundamental from the HHG supercontinuum and the samples. The spectral data is then captured on an X-ray charged coupled device (CCD) camera. By inserting and removing the samples, the spectrally-resolved absorptivity can be determined with high accuracy and analyzed with the software programs Athena and Artemis [38]. The spectrometer wavelength scale is calibrated using multiple characteristic absorption features and edges of thin film filters.

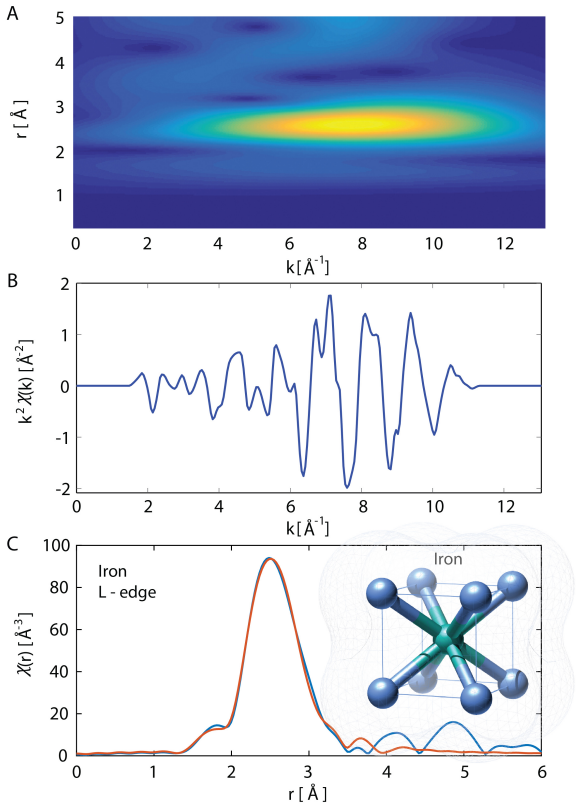

Figure 2. Experimental XAFS spectroscopy of a Fe thin film using 4 μm driving laser (orange soft X-ray spectrum from Fig. 1). **A)** CCWT analysis (modulus) near the Fe L-edge (0.7 keV); **B)** k^2-scaled EXAFS function in k-space extending to 12 Å^{-1}. **C)** Experimental real-space EXAFS function (blue), uncorrected for δ phase shifts, with first peak fitted (red) to theory. Inset shows a Fe bcc unit cell.

EXAFS is a universal response of matter interacting with X-ray light near an absorption edge. This quantum phenomenon can be understood in a simple three-step model, where an incident X-ray photon is absorbed by an atom, which leads to the ejection of a photoelectron from a core-shell. Then the photoelectron is scattered from neighboring non-excited atoms, and the quantum interferences of the outgoing and incoming scattered electron waves lead to an energy-dependent variation of the X-ray absorption probability (Figure 1C). In addition, these modulations are enriched by secondary and higher-order rescatterings that are also imprinted in the absorption or fluorescence spectra.

For EUV - X-ray pulses longer than 10 attoseconds, the maximum distance that can be probed through XAFS is limited by the mean free path of the electron (10-20 Å). For shorter HHG pulses (<10 as) this distance is expected to be significantly reduced. This limitation arises from the

fact that the HHG photon needs to be present at the absorbing atom during the electron scattering events in order to see a modulated absorption probability, and in general photons travel faster than electrons.

Figure 2B shows the experimentally extracted EXAFS function at the L-absorption edges (~700eV) of a monoatomic body-centered-cubic (bcc) Fe thin foil at room temperature, both in *k*-space and in real space.

These data were taken using a HHG supercontinuum source spanning from EUV to 1.6 keV, and the data is analyzed using the Athena and Artemis software [38]. A straightforward method for obtaining spatial distributions correlated to the interatomic distances is to take a Fourier transform of the *k*-scaled EXAFS function (Figures 2B and C). Fitting the first peak of spatial data to theory, we extract a nearest first shell distance of 2.48±0.03 Å (eight-fold degenerate) and second shell distance of 2.87±0.03 Å (six-fold degenerate), the latter value also being the lattice constant for a body centered cubic (bcc) crystal structure. Independent X-ray diffraction measurements affirm a bcc structure with a lattice constant of 286.68±0.03 pm for this sample. Peaks from multiple rescattering paths can be difficult to distinguish in general, and we use continuous Cauchy wavelet transform (CCWT) to decompose the EXAFS amplitude terms in real and reciprocal space (Figure 2A) [39]. Such a 2D plot can provide information for the *k* and *R* range of each nearest neighbor shell contribution and discriminate the shell distances for complex systems (Figure 2C).

The HHG supercontinuum driven by $\lambda = 2.1\,\mu m$ pulses do not extend to as high photon energies compared to the 4 μm laser; however, they are well suited for soft X-ray spectroscopy of importance for chemical and biological studies ('water window' region), as well as for investigation of phase transitions in inorganic materials such as VO_2, of interest for fast optical modulators and data storage devices. Here, extracting structural information from the EXAFS data leads to larger uncertainties since the *k*-range, over which the data is recorded, is limited to below 5-6 $Å^{-1}$. Nevertheless, these spectra are well suited for NEXAFS spectroscopies without the need of wavelength scanning. Figure 3 shows the absorption coefficient and the *R* and *k*-space EXAFS function distributions for a monoatomic Sc thin foil at the L-absorption edge (~398 eV). Our data is in excellent agreement with the CXRO database [40]. Fitting the spatial distribution data (Figure 3 C), we obtain a nearest first shell distance of 3.25±0.05 Å (six-fold degenerate) and the second shell distance of 3.30±0.05 Å (six-fold degenerate), in good agreement with the expected interatomic length.

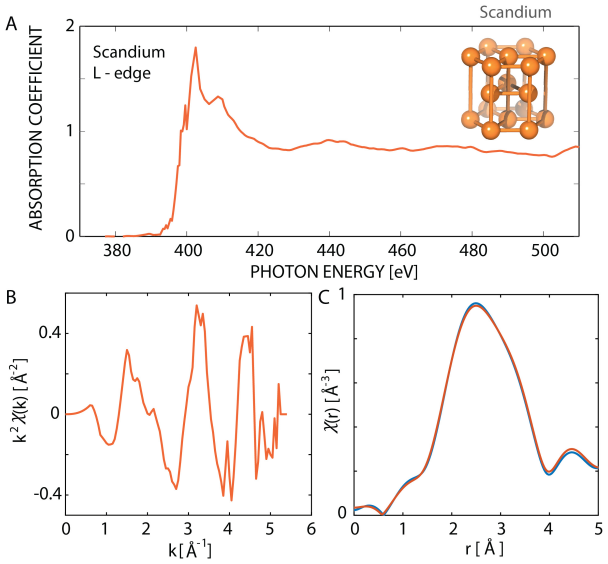

Figure 3. Experimental XAFS spectroscopy near the Sc L-edge, using a 2 μm -driven HHG supercontinuum up to 550 eV. **A)** The normalized absorption coefficient of Sc near the L-absorption edge at 398 eV. **B)** k^2-scaled EXAFS function in *k*-space extending to > 5 $Å^{-1}$. **C)** Experimental *R*-space EXAFS function (blue), not corrected for δ phase shifts, and fitted (red) to theory. The real space EXAFS function exhibits a broad peak. Inset shows a Sc hcp unit cell.

Coherent X-ray spectroscopies have an important additional advantage of being able to uncover the excited -state dynamics with elemental specificity, i.e., oxidation state, magnetic state, or charge localization to specific elements, giving information about the electronic structures, (i.e., valence, bands and charge), as well as orbital and spin ordering phenomena. The spectral features near an absorption edge are dictated by the atomic orbital overlap and the valence of the atoms. Modulations in the absorption spectra within 50 eV of an edge are labeled as near-edge X-ray absorption fine structure (NEXAFS). This X-ray bandwidth requirement is readily achieved by mid-IR-driven HHG supercontinua, and the optimal driving laser wavelength can be chosen for a phase-matched HHG cutoff energy moderately higher than the absorption edge energy [10, 12, 41]. For experiments near the chemically-relevant carbon K-edge at 284.2 eV, this prescribes a driving laser wavelength of $\lambda \sim 1.3\text{-}1.6\,\mu m$. Tuning the signal beam from a mid-IR OPA to $1.5\,\mu m$, the HHG X-ray supercontinuum is centered near ~300 eV, with a bandwidth of >180 eV. Figure 4 compares the near-edge absorption structures of mylar and parylene at the carbon K-absorption edge. These data show that we can resolve energy shifts as small as 0.2 eV in the 1s-π^* and 1s-σ^* absorption peaks, due to the sensitivity to the different molecular functional groups. The resolution in these measurements is close to 0.2 eV or $\lambda/\Delta\lambda \sim 1400$. Each spectrum was recorded for 0.05 sec (50 laser shots),

averaged over 30 exposures; in principle, these XAFS could be obtained in a single-shot mode. We identify transitions from 1s (K shell) to the antibonding π^* orbital (1s to π^*) of unsaturated C=C bonds of the aromatic ring near 285 eV [42]. The large peak at 285 eV shows predominantly unsaturated C bonds (i.e. sp^2 hybridization). The peak around ~289 eV is generally considered to be a mixed state of 1s to the antibonding σ^* orbital and 1s-3p (Rydberg-like) orbitals of the aromatic ring structure (Figure 4B) [42].

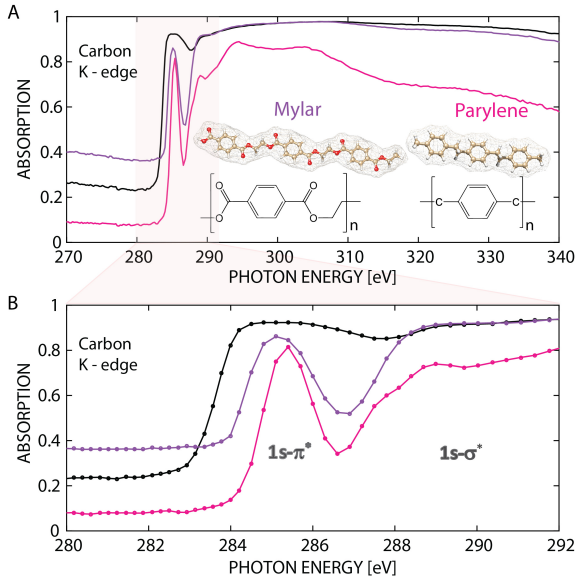

Figure 4. Experimental NEXAFS spectroscopy near the carbon K-edge using a 1.5 µm -driven HHG supercontinuum up to 360 eV. **A)** NEXAS of C-containing polymers (mylar (violet) and parylene (pink)), at the C K-edge. Also plotted is the experimental absorption spectrum of a carbon thin film (black) for reference. (Inset) Molecular structure of mylar and parylene rendered for trimers (C atoms in brown, O in red, H in white). **B)** Close-up view showing peaks due to transitions from 1s to both π^* and σ^* orbitals.

NEXAFS taken with polarized X-ray light are also sensitive to molecular orientation. For the 1s spherically symmetric initial state and polarized final state, the transition intensity is proportional to the $\cos^2(\vartheta_{\vec{\varepsilon},\vec{\lambda}_f})$, where $\vartheta_{\vec{\varepsilon},\vec{\lambda}_f}$ is the angle between the polarization of the electric field ($\vec{\varepsilon}$) and the direction ($\vec{\lambda}_f$) of the final orbital (Figure 1B), and is maximized when the polarization is parallel to $\vec{\lambda}_f$. In our experiment $\vec{\varepsilon}$ lies in the plane of the sample.

In summary, using coherent high-order harmonic broadband X-ray supercontinua generated by mid-IR lasers, we demonstrate first extended edge absorption spectroscopy (coherent EXAFS) at the K- and L-edges of elements at near-keV photon energies using a tabletop-scale apparatus. We also demonstrate near-edge soft X-ray absorption spectroscopy in the water window spectral region (coherent NEXAFS).

Finally, the unique temporal coherence of the HHG source – since the HHG emission in these spectral regions is in the form of a single sub-femtosecond chirped burst – opens the path for capturing coupled charge, spin and structural dynamics with femtosecond-to-attosecond time resolution and picometer spatial resolution. With some prior knowledge, these techniques can provide extensive spatio-temporal and chemical imaging information (4+1D) of the local atomic structure of materials, including 1) the types of atoms that are present, coordination numbers (number of neighboring atoms at particular distances), inter-atomic distances, as well as disorder (using EXAFS), and 2) the oxidation state, and coordination chemistry (i.e., symmetries, isomerism, etc.) (using NEXAFS) [35].

Acknowledgements

M.M and H.K. acknowledge support from the Department of Energy BES Award DE-FG02-99ER14982 (experiment) as well as a MURI grant from the Air Force Office of Scientific Research under Award Number FA9550-16-1-0121 (theory). B.R.G. gratefully acknowledges support from the National Nuclear Security Administration Stewardship Science Graduate Fellowship program. C.A.M. acknowledges support from the National Science Foundation Graduate Research Fellowship under Grant No. DGE 1144083.

* Margaret.Murnane@colorado.edu
* Tenio.Popmintchev@physics.ucsd.edu
Physics Department, University of California San Diego, La Jolla, CA 92093
* Dimitar.Popmintchev@gmail.com

[1] M. H. Key and R. J. Hutcheon, in *Advances in Atomic and Molecular Physics*, edited by R. B. David, and S. Benjamin Bederson (Academic Press, 1980), pp. 201.
[2] H. C. Gerritsen, H. van Brug, M. Beerlage, and M. J. Van der Wiel, Nuclear Instruments and Methods in Physics Research Section A: Accelerators, Spectrometers, Detectors and Associated Equipment **238**, 546 (1985).

[3] D. E. Sayers, E. A. Stern, and F. W. Lytle, Physical Review Letters **27**, 1204 (1971).
[4] L. Miaja-Avila *et al.*, Physical Review X **6**, 031047 (2016).
[5] R. Ian, G. Gerhard, and M. Simon, New Journal of Physics **12**, 035002 (2010).
[6] A. Rundquist, C. G. Durfee, Z. H. Chang, C. Herne, S. Backus, M. M. Murnane, and H. C. Kapteyn, Science **280**, 1412 (1998).
[7] E. J. Takahashi, T. Kanai, K. L. Ishikawa, Y. Nabekawa, and K. Midorikawa, Physical Review Letters **101**, 253901 (2008).
[8] T. Popmintchev, M. C. Chen, O. Cohen, M. E. Grisham, J. J. Rocca, M. M. Murnane, and H. C. Kapteyn, Optics Letters **33**, 2128 (2008).
[9] T. Popmintchev, M. C. Chen, A. Bahabad, M. Gerrity, P. Sidorenko, O. Cohen, I. P. Christov, M. M. Murnane, and H. C. Kapteyn, Proceedings Of The National Academy Of Sciences Of The United States Of America **106**, 10516 (2009).
[10] M. C. Chen, P. Arpin, T. Popmintchev, M. Gerrity, B. Zhang, M. Seaberg, D. Popmintchev, M. M. Murnane, and H. C. Kapteyn, Physical Review Letters **105**, 173901 (2010).
[11] T. Popmintchev, M. C. Chen, P. Arpin, M. M. Murnane, and H. C. Kapteyn, Nature Photonics **4**, 822 (2010).
[12] T. Popmintchev *et al.*, Science **336**, 1287 (2012).
[13] C. Ding, W. Xiong, T. Fan, D. D. Hickstein, T. Popmintchev, X. Zhang, M. Walls, M. M. Murnane, and H. C. Kapteyn, Optics Express **22**, 6194 (2014).
[14] K. Kaneshima, N. Ishii, T. Kanai, S. Watanabe, and J. Itatani, in *CLEO: 2015 Postdeadline Paper Digest* (Optical Society of America, San Jose, California, 2015), p. JTh5C.2.
[15] S. Cousin, F. Silva, S. Teichmann, M. Hemmer, B. Buades, and J. Biegert, Optics letters **39**, 5383 (2014).
[16] Y. Pertot *et al.*, Science **355**, 264 (2017).
[17] A. R. Attar, A. Bhattacherjee, C. D. Pemmaraju, K. Schnorr, K. D. Closser, D. Prendergast, and S. R. Leone, Science **356**, 54 (2017).
[18] M. E. Siemens, Q. Li, R. G. Yang, K. A. Nelson, E. H. Anderson, M. M. Murnane, and H. C. Kapteyn, Nature Materials **9**, 26 (2010).
[19] K. M. Hoogeboom-Pot *et al.*, PNAS **112**, 4846 (2015).
[20] S. Mathias *et al.*, Proceedings of the National Academy of Sciences of the United States of America **109**, 4792 (2012).
[21] C. La-O-Vorakiat *et al.*, Physical Review X **2**, 011005 (2012).
[22] C. La-O-Vorakiat *et al.*, Physical Review Letters **103**, 257402/1 (2009).
[23] D. Rudolf *et al.*, Nature Communications **3**, 1037, 1037 (2012).
[24] E. Turgut *et al.*, Physical Review Letters **110**, 197201 (2013).
[25] Z. Tao, C. Chen, T. Szilvási, M. Keller, M. Mavrikakis, H. Kapteyn, and M. Murnane, Science **353**, 62 (2016).
[26] C. Chen *et al.*, Proceedings of the National Academy of Sciences, 201706466 (2017).
[27] M.-C. Chen *et al.*, Proceedings of the National Academy of Sciences of the United States of America **111**, E2361 (2014).
[28] E. Seres, J. Seres, and C. Spielmann, Applied Physics Letters **89**, 181919 (2006).
[29] E. Seres, J. Seres, and C. Spielmann, Applied Physics A **96**, 43 (2009).
[30] P. A. Lee, P. H. Citrin, P. Eisenberger, and B. M. Kincaid, Reviews of Modern Physics **53**, 769 (1981).
[31] G. Bunker, National Biostrustures PRT, unpublished http://gbxafs.iit.edu/training/Noise.pdf (1988).
[32] *European XFEL http://www.xfel.eu/*.
[33] N. R. Council, *Controlling the quantum world: the science of atoms, molecules, and photons* (National Academies Press, 2007), Vol. 2.
[34] *Slac https://heds.slac.stanford.edu/our-research/record-peak-brightness*.
[35] D. Popmintchev, *Quantum and Extreme Nonlinear Optics Design of Coherent Ultrafast X-ray Light and Applications, Thesis* (ASIN: B01N9G9JVZ, 2016).
[36] S. Teichmann, F. Silva, S. Cousin, M. Hemmer, and J. Biegert, Nature communications **7** (2016).
[37] G. Andriukaitis, T. Balciunas, S. Alisauskas, A. Pugzlys, A. Baltuska, T. Popmintchev, M. C. Chen, M. M. Murnane, and H. C. Kapteyn, Optics Letters **36**, 2755 (2011).
[38] B. Ravel and M. Newville, Journal of Synchrotron Radiation 537 (2005).
[39] M. Muñoz, F. Farges, and P. Argoul, Physica Scripta **2005**, 221 (2005).
[40] C. http://henke.lbl.gov/.
[41] D. Popmintchev *et al.*, Science **350**, 1225 (2015).
[42] Y. Ma, H. Yang, J. Guo, C. Sathe, A. Agui, and J. Nordgren, Applied Physics Letters **72**, 3353 (1998).
[43] See Supplemental Material [url], for raw and analyzed data and methods used to estimate the HHG properties in the main text, which includes Refs. [44-50].
[44] D. Popmintchev et al., Science **350**, 1225 (2015).
[45] D. Popmintchev, Quantum and Extreme Nonlinear Optics Design of Coherent Ultrafast X-ray Light and Applications, Thesis (ASIN: B01N9G9JVZ, 2016).
[46] Q. Shen, X-ray flux, brilliance and coherence of the proposed Cornell energy-recovery synchrotron source, 2001.
[47] P. Shukla, J. Lawrence, and Y. Zhang, Optics & Laser Technology **75**, 40 (2015).
[48] European XFEL http://www.xfel.eu/.

[49] N. R. Council, Controlling the quantum world: the science of atoms, molecules, and photons (National Academies Press, 2007), Vol. 2.
[50] Slac https://heds.slac.stanford.edu/our-research/record-peak-brightness.